Applied Energy 332 (2023) 120546

Contents lists available at ScienceDirect

Applied Energy

journal homepage: www.elsevier.com/locate/apenergy

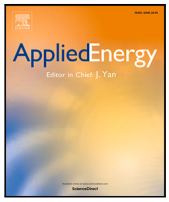

CO_2-plume geothermal: Power net generation from 3D fluvial aquifers

Amir Mohammad Norouzi [a,*], Fatemeh Pouranian [b], Arash Rabbani [c], Neil Fowler [d], Jon Gluyas [d,e], Vahid Niasar [a], Justin Ezekiel [f], Masoud Babaei [a,d,**]

[a] Department of Chemical Engineering, The University of Manchester, Manchester, UK
[b] Energy, Water, and Environment Research Center, School of Mechanical Engineering, Iran University of Science and Technology, Tehran, Iran
[c] School of Computing, University of Leeds, UK
[d] Shift Geothermal Ltd, UK
[e] The Department of Earth Sciences, Durham University, UK
[f] Physical Science and Engineering Division, King Abdullah University of Science and Technology, Thuwal 23955-6900, Saudi Arabia

ARTICLE INFO

Keywords:
CO_2-plume geothermal
Thermosiphon
Heterogeneity
Fluvial channels
Geothermal power

ABSTRACT

Previously CO_2, as a heat-extraction fluid, has been proposed as a superior substitute for brine in geothermal energy extraction. Hence, the new concept of CO_2-plume geothermal (CPG) is suggested to generate heat from geothermal aquifers using CO_2 as the working fluid. In January 2015, a CPG-thermosiphon system commenced at the SECARB Cranfield Site, Mississippi. By utilizing CO_2, the demand for the pumping power is greatly reduced due to the thermosiphon effect at the production well. However, there are still parameters such as aquifer thermal depletion, required high injection rates, and CO_2-plume establishment time, that hinder CPG from becoming viable. Moreover, the fluvial nature of sedimentary aquifers significantly affects the heat and mass transfer inside the aquifer, as well as the system performance. In the present study, a direct-CO_2 thermosiphon system is considered that produces electricity from a 3D braided-fluvial sedimentary aquifer by providing an excess pressure at the surface that is used in the turbine. The system performance and net power output are analysed in 15 3D fluvial heterogeneous – with channels' widths of 50, 100, and 150 m – and three homogeneous aquifer realizations with different CO_2 injection rates. It is observed that the presence of fluvial channels significantly increases the aquifer thermal depletion pace (22%–120%) and therefore, reduces the system's performance up to about 75%. Additionally, it is found that the CPG system with the CO_2 injection rate of 50 kg/s and the I-P line parallel to the channels provides the maximum cycle operation time (44 years), as well as the optimum performance for the heterogeneous cases of the present study by providing about 0.06–0.12 TWh energy during the simulation time of 50 years. Also, to prevent rapid drops in excess pressure, a system with a yearly adjustable injection rate is implemented, which prevents the production well bottomhole temperature to fall below 80 °C.

1. Introduction

About 41% of global (25% of the UK) carbon dioxide (CO_2) emissions from fossil fuel combustion in 2017 are due to electricity and heat production activities [1]. Now, more than ever, the importance of reducing global CO_2 emissions has become evident. Several measures have been taken to tackle this problem, among which, CO_2 capture and storage (CCS) is the most considered and noted one [2–4]. Instead of only storing CO_2 in underground formations, CO_2 can be circulated to the surface and used in carbon capture utilization and storage (CCUS) systems, such as enhanced oil recovery (EOR) [5–7], enhanced gas recovery (EGR) [8,9], and heat extraction in enhanced geothermal systems (EGS) [10–12].

Recently, CO_2 is suggested as a substitute for water for geothermal power generation in naturally permeable sedimentary formations, known as CO_2-plume geothermal (CPG) process [13], and in 2015, a CPG-thermosiphon system started at the SECARB Cranfield Site, Mississippi [14]. In CPG power generation, CO_2 is injected and produced in the supercritical (sc) phase. During this cycle of geothermal power generation, all of the produced CO_2 is re-injected into the aquifer, and eventually, all of the initially injected CO_2 will be kept in the underground aquifer.

Using CO_2 features three main advantages, *i.e.*, (i) self-sustaining thermosiphon effect, (ii) lower frictional losses, and (iii) grid-scale

* Corresponding author.
** Corresponding author at: Department of Chemical Engineering, The University of Manchester, Manchester, UK.
E-mail addresses: amirmohammad.norouzi@manchester.ac.uk (A.M. Norouzi), masoud.babaei@manchester.ac.uk (M. Babaei).

https://doi.org/10.1016/j.apenergy.2022.120546
Received 29 August 2022; Received in revised form 24 November 2022; Accepted 18 December 2022
Available online 27 December 2022

electricity storage [15,16]. Unlike water, CO_2's density is highly temperature-dependent. This results in a considerable drop in its density while it is heated inside the aquifer, resulting in an upward flow from the density-driven thermosiphon effect [17]. Additionally, CO_2's lower viscosity results in lower frictional losses and pressure drop inside the aquifer. Therefore, higher flowrates (with the same amount of pressure drop) compared to water-based systems are possible. Moreover, because of the CO_2's higher compressibility, it is possible to provide grid-scale electricity storage [18].

Since the introduction of CPG, there have been some studies on the performance and thermal potential assessment of CPG sites, as well as studies on different aspects of the CPG systems. The most recent of these studies are about minerals precipitation [19–21], wells' spacing [15,22], well pattern and reservoir boundary condition [23], surface power plant cycle [16,24,25], water and $scCO_2$ saturation and mass-fraction at the production well [26,27], CPG combination with natural gas recovery [9], and CPG economic feasibility [24].

CPG typically is recommended for relatively shallow sedimentary aquifers with depths of about 0.5 km to 3 km [17]. Compared to fractured formations, sedimentary aquifers are naturally porous and permeable and are abundant worldwide [28–30]. As noted by Bonté et al. [31], there are many low-enthalpy geothermal aquifers available with depths of 2–2.5 km and an average temperature of 70–90 °C. Heterogeneity is the nature of all geological aquifers, and in sedimentary brine aquifers (that are used for CPG), these heterogeneities can be of the fluvial type, *i.e.*, braided, meandering, and anabranching [32]. Fluvial sandstones are common as reservoirs for both water and hydrocarbon. Examples include the Triassic strata and significant parts of the Permian section in Europe including the Triassic Sherwood Sandstone of the Worcester Graben, Wessex, Cheshire and East Irish Sea Basins, UK [33,34], the Triassic Bunter Sandstone of the UK and Dutch Southern North Sea, North German Basin [35,36], Permo-Triassic sandstone reservoirs of the Junggar Basin China [37], Devonian sandstones at Battery Point Quebec [38], and more [39].

Our previous study showed that the presence of fluvial channels in the aquifer affects the heat and mass dispersion inside the aquifer and therefore, significantly affects the performance and the energy output of CPG [22]. However, despite the importance of geological uncertainty in modelling such systems, there are few studies that considered realistic three-dimensional (3D) models of heterogeneity [40–44]. Most of these works focused on CCS and water-based systems, rather than CPG. In our previous study [22], the performance of a CPG system in a two-dimensional (2D) braided fluvial aquifer was investigated through subsurface performance metrics. It was observed that the injection-production wells parallel to fluvial channels direction and with the spacing of about 450 m provides the best system performance. Moreover, the presence of fluvial heterogeneity reduced the system net power by a factor of 3. The study had some limitations. The model was 2D and could not capture the density-driven upstream flow of $scCO_2$ inside the aquifer. Additionally, the performance of the system was analysed based on subsurface metrics only and thermosiphon was not considered.

In addition to heterogeneity, the aquifer thermal depletion and variations of aquifer temperature during the CPG lifetime is also mostly overlooked in studies in this field. Among the works that considered the reservoir heat depletion [9,45,46], and [47] can be mentioned. Most recently, Adams et al. [15] considered the reservoir thermal depletion and suggested a system working with the optimal flowrate at each time step. However, the issue with this approach is that, in practice, it is not possible to instantly adjust the injection rate every time step. Also, due to the large volume of the reservoir, the system has a response time regarding the variations in flowrate.

Despite the importance of geological uncertainty and aquifer heat depletion, there is no study on 3D heterogeneous aquifer, with a direct-CO_2 thermosiphon power generation cycle. Against this backdrop, we focus on realistic 3D heterogeneity of aquifers and how they affect the efficiency and performance of CPG, thermosiphon and power generation. A fully heterogeneous braided fluvial 3D aquifer is considered for a direct-CO_2 thermosiphon system. Various fluvial realizations are created and the results are compared with their representative homogeneous cases. In addition to the aquifer and well modelling, a direct-CO_2 expansion turbine is considered at the surface power plant for power generation. Also, effects of various parameters such as fluvial channels' width and orientation and CO_2 injection rate are studied and an optimum injection rate for heterogeneous and homogeneous cases is suggested. Finally, a CPG system with an annually adjusting injection rate is suggested to keep the produced excess pressure at the surface (associated with thermosiphon) constant during the cycle lifetime.

2. Methods

To model the CPG system as realistically as possible, several aspects of the CPG cycle should be considered, including modelling fluid flow and heat transfer in the aquifer, fluid transfer from bottomhole condition to the surface, and energy production at the surface power plant. Each of these is described in the following sections.

2.1. Aquifer and well modelling

A 3D rectangular Cartesian aquifer with the domain of 1000 m × 1000 m × 100 m at the depth of 2000 m is modelled for 50 years of heat extraction. The aquifer is initially uniformly discretized into 400 × 400 × 25 grid blocks and then upscaled to a model of 50 × 50 × 25 grid blocks to reduce the simulations' time [22]. Grid resolution sensitivity results are provided in Section 2.4. Based on the optimized results provided in a previous study [22], a pair of vertical injection (I) and production (P) wells with the spacing of $L = 500$ m and the I-P line parallel to the channels' orientation is considered to provide the highest performance. However, to further study the effect of the I-P line and channels' orientation, the performance of CPG systems with the I-P line perpendicular to channels is compared with cases with the I-P line perpendicular to channels in Section 3.1. The injection and the production wells are perforated at the lower and the upper halves of the aquifer, respectively.

The aquifer is designed based on the data from Warren et al. [48] and previous publications, particularly [21–23,49], to represent a high-salinity North Sea sandstone aquifer. Although salt precipitation, due to water vapourisation in the dry-out region, and geochemical reactions take place in the reservoir, it was previously shown that the main reaction is salt precipitation, with effects limited to the close vicinity of the injection well. Despite the increase in the pressure drop inside the reservoir due to salt precipitation, its effects on the system's thermal performance are small [21–23,50]. However, to further investigate this matter, a sensitivity analysis on the effects of geochemical reactions, specifically salt, is provided in Appendix. Additionally, the effects of the fluvial channels' permeability and porosity, as well as the injection well bottomhole temperature are studied in this section.

The aquifer is initially filled with brine with a salinity of 20% by weight. The initial pressure equates to the hydrostatic elevation potential at the aquifer depth which will be about 20 MPa at the aquifer's top. Also, the aquifer initial temperature is the product of the temperature gradient (42.5 °C km^{-1}) and the aquifer depth plus the ambient temperature (15 °C), which will be about 100 °C. Because of the caprock and bedrock at the top and bottom of the aquifer, the vertical boundaries of the aquifer are closed to flow. However, conductive heat exchange happens at the boundaries. Pore volume modification is used at the side boundaries to represent an aquifer with side boundaries open to flow and heat transfer. The aquifer is modelled using two-phase flow simulations of CO_2 and brine with varying temperature and pressure, and the Peng–Robinson [51] Equation of State is used to calculate the thermodynamic properties of each phase. Detailed aquifer properties are provided in Table 1.

Table 1
Aquifer properties.

Property	Value
Aquifer properties: constant	
Aquifer domain	1000 m × 1000 m × 100 m
Depth	2000 m
Salinity	20 wt.-%
Initial temperature	100 °C
Initial top pressure	20 MPa
Channels' width to thickness ratio (w/T)	10
Channels' porosity	0.25
Inter-channels' porosity	0.15
Channels' horizontal permeability	1000 mD
Inter-channel's horizontal permeability	20 mD
Vertical to horizontal permeability ratio	0.1
Rock density	2650 kg/m^3
Rock heat capacity	1987.5 kJ/m^3/K
Rock thermal conductivity	2.1 W/m/K
Bottomhole injection temperature	40 °C
Wellbore diameter	0.31 m
Well pipe surface roughness	55 μm
Aquifer properties: varied	
Injection rate ($\dot{m}_{inj}$)	5, 10, 25, 50[a], 100, and 200 kg/s
Fluvial channels' width (w)	50[a], 100, and 150 m
Homogeneous average porosity (ϕ)	0.17[a], 0.185, and 0.208
Homogeneous average permeability (k_{avg})	225.5[a], 336.5, and 568.4 mD
I-P wells' orientation with respect to channels	parallel[a] and perpendicular

[a]Indicates the base case parameters.

The pressure drop for a steady and laminar flow inside the aquifer can be calculated using Darcy's equation [52]. The term inside the bracket in Eq. (1) is the average specific inverse mobility (M) that is the product of the kinematic viscosity (μ/ρ) and the aquifer-dependent properties ($L/k/A$) and shows the aquifer's resistance to flow. Since the aquifer permeability is not constant, and scCO$_2$'s density and viscosity are temperature dependent, it is not possible to directly calculate M, however, knowing the injection rate and the pressure drop from the aquifer simulations, M can be calculated. It is assumed that the fluvial channels and heterogeneity reduce the aquifer mobility and therefore, increase the required pumping power. This parameter will be used in future sections to optimize the CO$_2$ injection rate at each time step.

$$\Delta P = \left[\frac{\mu L}{\rho k A}\right]\dot{m} \tag{1}$$

It is assumed that CO$_2$ goes through isentropic (adiabatic and reversible) compression and expansion processes in the injection and production wells, respectively [15]. To model the injection and the production wells and to calculate CO$_2$'s temperature and pressure at the surface and bottomhole conditions, wells are divided into segments of 50 m to reach an accuracy within 1% of the values found through a fine-scale model. The injection temperature of CO$_2$ (T_{inj} = 40 °C) is calculated by isentropically compressing the injected saturated liquid CO$_2$ at T = 22 °C and P = 6 MPa at the surface to the supercritical phase at the aquifer pressure. Similarly, at the production wells, knowing the bottomhole temperature and pressure, the CO$_2$ temperature and pressure are calculated through numerical well modelling, considering an isentropic expansion. A schematic of the modelled CPG aquifer is illustrated in Fig. 1.

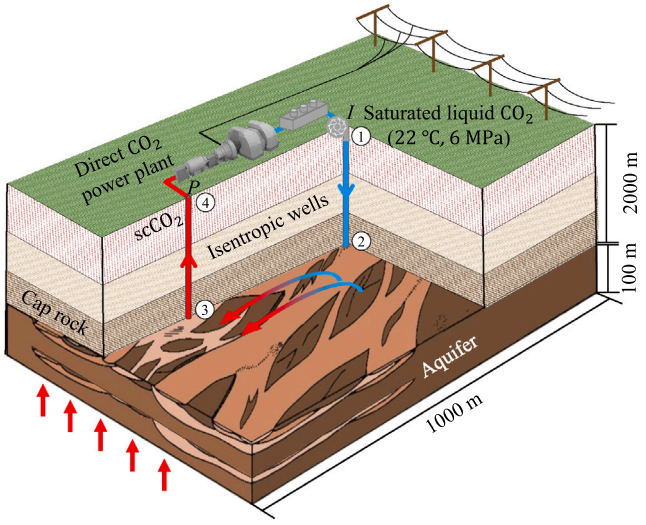

Fig. 1. Schematic of the direct-CPG cycle and surface power plant. The turbine's isentropic efficiency (η_T) is considered to be 78%.

2.2. Sequestration stage vs. CPG lifetime

When CO$_2$ is injected into the aquifer, it initially displaces brine, a stage known as the CO$_2$-Plume Establishment (PE) stage. Having a sufficient amount of CO$_2$ in the aquifer is crucial; otherwise, once the production begins, water will emerge at the production well. At this stage, the CO$_2$ mass-fraction is too low and cannot be used in a turbine for energy production. However, Ezekiel et al. [26] suggested that in light of the CO$_2$'s lower viscosity compared to brine, only when CO$_2$ saturation around the production well is higher than about 0.3, the influx of CO$_2$ into the well is much higher than the water. Hence, to sustain a desirable *annular* production flow regime (as suggested by Ezekiel et al. [26]), a minimum CO$_2$ mass-fraction of 80% is considered for the onset of energy production and the CPG cycle [15,26,45]. In the present work, the required time interval for this stage is called the *sequestration stage*.

Furthermore, it is essential that the produced CO$_2$ at the surface (stage 4 in Fig. 1) is still at its supercritical condition; thus, a shutdown trigger is considered at the production well that stops power production when either the temperature or the pressure of the produced CO$_2$ fall below its critical point of 30.3 °C and 7.38 MPa, which defines the *CPG lifetime*. The span between the sequestration stage and CPG lifetime is the cycle *operation time*. Finally, one of the major concerns in CPG is the production temperature drop, which weakens thermosiphon, reduces power production, and shortens the CPG lifetime. To non-dimensionalize the production temperature and temperature decay, a

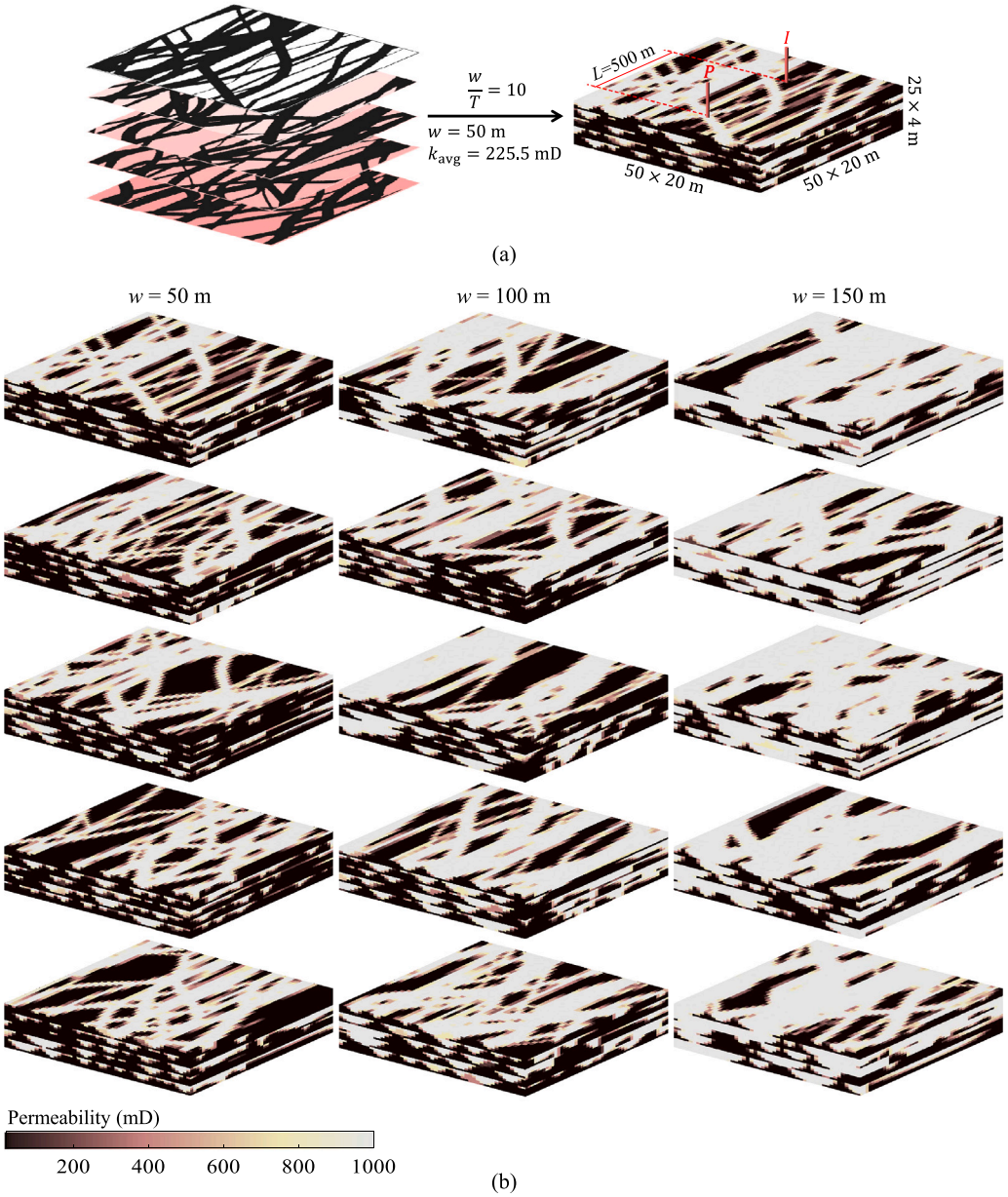

Fig. 2. (a) Schematic of the problem and the aquifer (w = 50 m); and (b) heterogeneous cases with 15 different realizations, (left): w = 50 m and k_{avg} = 225.5 mD, middle: w = 100 m and k_{avg} = 336.5 mD, and right: w = 150 m and k_{avg} = 568.5 mD.

temperature fraction parameter (Γ) is defined:

$$\Gamma_t = \frac{T_t - T_{inj}}{T_0 - T_{inj}} \tag{2}$$

where T_t is the production bottomhole temperature at time t, T_0 is the aquifer initial temperature (100 °C), and T_{inj} is the $scCO_2$ injection temperature (40 °C).

2.3. Fluvial channels

There are different types of fluvial channels, including straight, meandering (e.g., Cretaceous Nieuwerkerk Formation, West Netherlands Basin [53]), and braided (e.g., Bunter sandstone reservoir, UK; Tarim basin, China; the Triassic St Bees Sandstone Formation, Cumbria, UK [54]; and Sherwood Sandstone Group of the Wessex Basin, UK [34]). Generally, a single thread channel with a low degree of sinuosity (<1.5) is called straight and with a higher degree of sinuosity (>1.5) is called meandering [32]. Sinuosity is the ratio between the curvilinear length and the straight line connecting the curve's endpoints. The aquifer modelled in the present study has the subsurface fluvial channels of braided type. Braided channels have low sinuosity and consist of a network of channels with high porosity and permeability that are mostly (>50%) separated by scattered low porosity and permeability matrices [55,56]. The braided channels' degree of heterogeneity is defined by their channels' width and width-to-thickness ratio (w/T). Based on the review and the geological data provided by Gibling [57], channels' widths of 50, 100, and 150 m with the w/T ratio of 10 are considered to generate the fluvial realizations in this study (Fig. 2a).

In total, 15 randomly-created 3D braided aquifers are generated for this study (Fig. 2b). To generate these realizations, an in-house code that works based on the Piece-wise Cubic Hermite Interpolating Polynomials [58] is developed. To generate each 3D realization, at first, five layers of randomly generated 2D braided channels with a considered width, *i.e.*, w = 50, 100, and 150 m, are created. The process of creating 2D channels is described in our previous studies [22,59].

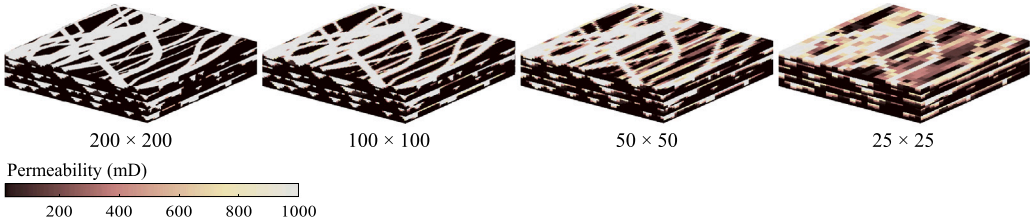

Fig. 3. Aquifer resolutions considered for the grid sensitivity analysis.

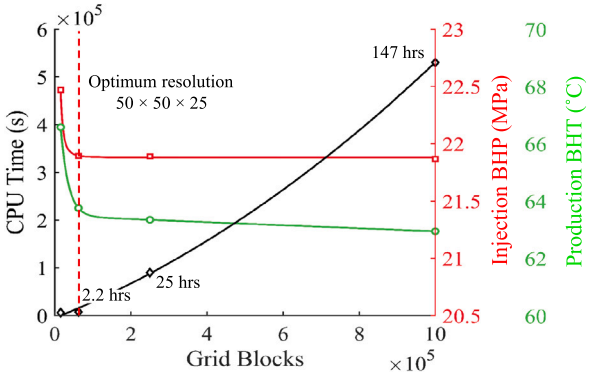

Fig. 4. Grid resolution sensitivity analysis: CPU time, production bottomhole temperature, and injection bottomhole pressure versus aquifer resolution.

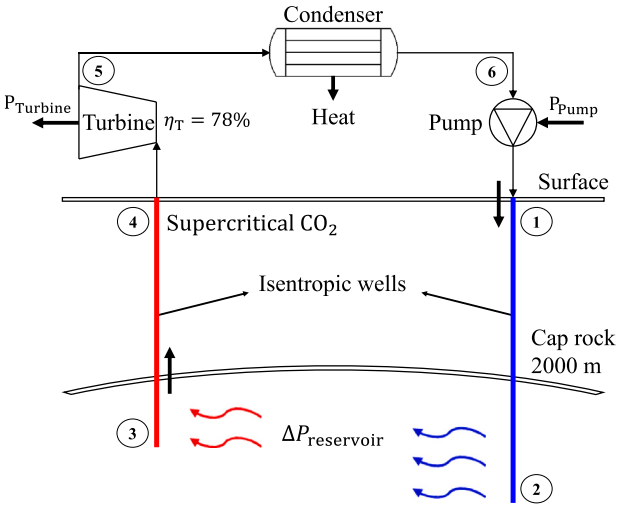

Fig. 5. Direct-CO_2 thermosiphon system.

Then, using the w/T ratio of 10, a thickness is assigned to all the channels. Next, these five braided realizations that now have a thickness, are put on top of each other to form a 3D braided aquifer. Finally, the initial fine-scale cases are upscaled to reach the final cases with 50 × 50 × 25 grid blocks, as shown in Fig. 2(b). To compare the homogeneous versus heterogeneous aquifers, a homogeneous case is created representing each channel width. For each homogeneous case, the average porosity and permeability are calculated by averaging the values of the volumetric-averaged porosity and permeability of the related heterogeneous cases.

To study the effects of mesh resolution on the subsurface results and find the optimum resolution both in terms of simulation runtime and results error, four resolutions, including 200 × 200 × 25, 100 × 100 × 25, 50 × 50 × 25, and 25 × 25 × 25 are considered, as in Fig. 3. The overall simulation CPU time, as well as the production well bottomhole temperature and the injection well bottomhole pressure, after 50 years of injection, are used to study the resolution effect.

Fig. 4 illustrates the grid resolution sensitivity analysis results. The simulations are performed on an HP ProLiant High Performance Server with two E5-2690v3 processors. The simulation runtime is increased with a logarithmic trend as the aquifer resolution is increased, while the variations in bottomhole temperature and pressure are negligible (less than 1 °C and 50 kPa). Therefore, considering both the runtime and the upscaling error, the optimized grid resolution for the present study is 50 × 50 × 25, which is similar to the results of the 2D model in our previous study [22].

2.4. Surface power plant modelling and flowrate optimization

In the present study, CO_2 is directly used as the working fluid of the power cycle and is expanded through a turbine to produce power. Therefore, a direct-CO_2 thermosiphon CPG system, comprised of an expansion turbine, a cooler/condenser heat exchanger, and a pump is used to generate electricity from the medium-temperature aquifer of the present study [9,17,60]. A schematic of this direct-CO_2 power cycle is shown in Fig. 5.

Saturated liquid CO_2 with a temperature and pressure within the ranges of 22–27 °C and 6.0–6.7 MPa, respectively, is injected into the reservoir (Fig. 5, stage 1). Then the injected CO_2, in an isentropic process, self-compresses inside the injection well and becomes supercritical as it reaches the aquifer condition at stage 2. As the scCO_2 is heated inside the aquifer from stage 2 to 3, its density considerably decreases. For instance, CO_2 density decreases from about 850 kg/m^3 at 40 °C (bottomhole injection temperature) to about 450 kg/m^3 at 100 °C (aquifer temperature). The compression and the expansion inside the wells are considered to be isentropic. As a result of the density gradient, the pressure difference between the bottom and top of the production well will be less than that of the injection well, *i.e.*, $|\Delta P_{3,4}| < |\Delta P_{1,2}|$. Hence, the aquifer bottomhole pressure itself is sufficient to produce the scCO_2 from the production well to the surface and no additional pump is required, resulting in an excess pressure ($P_{excess} = P_4 - P_1$) at the surface. P_{excess}, which is the difference between the production and injection wells' head pressure, shows that the produced fluid has higher exergy. The high-pressure sc/gaseous CO_2 that is produced from the aquifer is expanded in the turbine and using a generator, electric power (MW_e) is generated.

The gross turbine power (P_T) is calculated by multiplying the scCO_2 mass flowrate by the fluid enthalpy difference between the inlet (stage 4) and the outlet (stage 5) of the turbine (Δh). Eq. (3) is used to calculate P_T. Ideally, the expansion process inside the turbine is isentropic, however, because of irreversibilities, an isentropic turbine efficiency (η_T) of 78% is used to calculate the enthalpy at the turbine's exit as in Eq. (4).

$$P_T = X_{CO_2}\dot{m}(h_{in} - h_{out}) \tag{3}$$

$$h_{out} = h_{in} - [\eta_T(h_{in} - h_{out,s})] \tag{4}$$

In the above equations, X_{CO_2} is the produced CO_2 mass-fraction in the gas phase and $\dot{m}$ is the produced CO_2 mass flowrate in kg/s.

h_{in} is the inlet enthalpy of the turbine (stage 4), which is a function of the scCO$_2$ temperature ($T_{prod,head}$) and pressure ($P_{prod,head}$) at the production wellhead, and h_{out} represents the exit enthalpy of the turbine. $h_{out,s}$ is the enthalpy of the outlet CO$_2$ considering an ideal turbine (η_T = 100%) and is a function of the entropy of the inlet CO$_2$ (s_{in}) and the condenser pressure (P_{cond}). P_{cond} itself is a function of the condenser outlet temperature ($T_{out,cond}$), which is considered to be 7 °C above the ambient temperature ($T_{ambient}$ = 15 °C) [9,60]. Also, it is considered that the mass vapour quality of the fluid leaving the condenser is equal to zero ($Q = 0$), *i.e.*, CO$_2$ is in the liquid phase.

$$h_{in}, s_{in} = f(P_{prod,head}, T_{prod,head}) \tag{5a}$$

$$h_{out,s} = f(P_{cond}, s_{in}) \tag{5b}$$

$$P_{cond} = f(T_{out,cond}, Q) \tag{5c}$$

To calculate the net power (P_{net}) of the direct-CO$_2$ cycle, we should subtract the parasitic condenser power (P_{cond}) and pump power (P_{pump}) from the gross turbine power (P_T), as in Eq. (6).

$$P_{net} = P_{turbine} - P_{cond} - P_{pump} \tag{6}$$

In light of the thermosiphon effect, the required pumping power for a direct CPG cycle is equal to zero ($P_{pump} = 0$) [9,60], which is the main advantage of CPG compared to water-based systems. Electrical submersible pumps in wells are very expensive, and also, are the most common equipment to fail, increasing maintenance costs [61].

To calculate the parasitic condenser power (P_{cond}), Eq. (7) is used, in which, $h_{in,cond}$ and $h_{out,cond}$ represent the fluid enthalpy at the condenser inlet (stage 5) and exit (stage 6), respectively, and λ is the parasitic load fraction, which is the ratio of parasitic energy load to heat-rejection energy and is considered to be 0.03 [9].

$$P_{cond} = X_{CO_2} \dot{m}(h_{in,cond} - h_{out,cond})\lambda \tag{7}$$

One of the main issues in CPG systems is the temperature drop at the production well. When the injected scCO$_2$ thermal plume reaches the production well, its temperature greatly decreases, and therefore, weakens the thermosiphon at the production well. In addition, it is important to limit the pressure drop at the turbine's inlet during the CPG lifetime. In this regard, a set of simulations are designed where the aquifer parameters (*i.e.*, the aquifer pressure drop and inverse mobility M), are recalculated every year and the CO$_2$ injection rate is adjusted in a way to keep the production temperature and the excess pressure (P_{excess}) above a certain level at all times. To do so, first, we assume a lower limit for the excess pressure, then at time step i, we have the injection rate from time step $i-1$, so from Eq. (1) we can calculate the inverse mobility M. For time step $i+1$, the pressure drop is calculated by having the value of M, and knowing the updated pressure drop, the injection rate is adjusted. This process repeats every year to adjust the injection rate and prevent the bottomhole production temperature and the P_{excess} fall blow defined values of 80 °C and 3.5 MPa, respectively.

2.5. Simulations and the employed simulators

In total, 156 cases that include 18 different 3D aquifer realizations (5 heterogeneous and 1 homogeneous realization for each channel width) are simulated. For each realization, 6 different injection mass flowrates (5, 10, 25, 50, 100, and 200 kg/s) and a case with a time step-adjusted injection rate are considered. Additionally, 5 heterogeneous cases with the I-P line perpendicular to the channels' orientation are considered to study the effect of channels' orientation. All the simulations are carried out using the ECLIPSE E300 simulator [62], and the governing equations are detailed in [49,62]. The simulator's capability of modelling geothermal processes have been validated previously against the benchmark geothermal examples from Stanford University [63]. The authors proved that the simulator is suitable for use in complex geothermal modelling problems. Simpler adaptations of CPG have been implemented by other authors employing industry standard simulators such as CMG [26,60]. Additionally, the well and the direct-CO$_2$ power plant models are developed in MATLAB, and the CoolProp-MATLAB wrapper [64] is used for the iterative calculation of the fluid thermodynamic properties at each stage.

3. Results and discussion

Results are presented in two sections. First, a detailed comparison of the performance and the net power of the CPG system between the homogeneous and the heterogeneous fluvial cases is provided. To do the comparison, parameters including the temperature fraction, production wellhead temperature, the aquifer inverse mobility and production rate, cycle excess pressure, and instantaneous and cumulative net power, are studied in Section 3.1. Last, in Section 3.2, results of the cases with constant target excess pressure are presented and the CPG system potential is analysed and compared between the cases.

3.1. Effects of heterogeneity, injection rate, and channels' orientation on system performance

Fig. 6a and b show the temperature fraction and the wellhead temperature, as well as the cycle sequestration stage, versus time for the constant channels' width of 50 m. One of the main problems of CPG is the aquifer thermal depletion that weakens thermosiphon. Fig. 6a shows the sequestration stage (the length of the PE stage, at which the CO$_2$ pore-space saturation reaches about 0.3 or mass-fraction of about 80% around the production well). The scCO$_2$ injection rate significantly affects the required sequestration stage — from about 2 years to 37 years. Based on these results, CPG with a single pair of wells and low injection rates (such as 5 and 10 kg/s in this study) is not practical if used in brine-filled aquifers, because although the temperature drop is very low, the required sequestration stage will be more than 20 years, which is about 0.4 of the cycle's expected operation time (50 years). A solution to this issue can be using multiple injection and production wells in a pattern that they supplement each other's CO$_2$-plume to provide the minimum required mass-fraction at the production well. For higher injection rates, the sequestration stage is about 9, 5.5, 3, and 2 years for injection rates of 25, 50, 100, and 200 kg/s, respectively.

In Fig. 6b, the values of the production wellhead temperature are reported. It is observed that the temperature achieved at the surface – for the power plant use – has much lower values compared to the downhole ones. This is because CO$_2$ goes through an isentropic expansion in the production well that can reduce its temperature from about 100 °C to about 63 °C. The time at which either the temperature or the pressure of the produced CO$_2$ at the surface falls below the critical values of 30.3 °C and 7.38 MPa is the CPG lifetime. In contrast with the sequestration stage, as the injection rate increases, the aquifer thermal depletion occurs at a faster pace, and therefore, the CPG lifetime decreases on average about 17 and 38 years for the 100 kg/s and 200 kg/s injection rate cases, respectively (Fig. 6b). As a result, finding an injection rate that observes the balance between the sequestration stage and CPG lifetime is vital.

The presence of fluvial channels increases the slope of the curve for aquifer thermal depletion compared to homogeneous cases since the scCO$_2$ thermal plume reaches the production well faster (Fig. 6a and b). For instance, from Fig. 6c and d, for $\dot{m}_{inj}$ = 50 kg/s and w = 50 m, the amount of reduction in Γ ($\Delta\Gamma$) versus time increases from about 0.3 to 0.6. However, heterogeneity slightly affects the sequestration stage by about 1 to 6 years, depending on the injection rate. There are two observations when the channels' width increases from 50 m to 150 m. Firstly, the higher the channels' width is, the lower the difference between homogeneous and heterogeneous cases is. In other

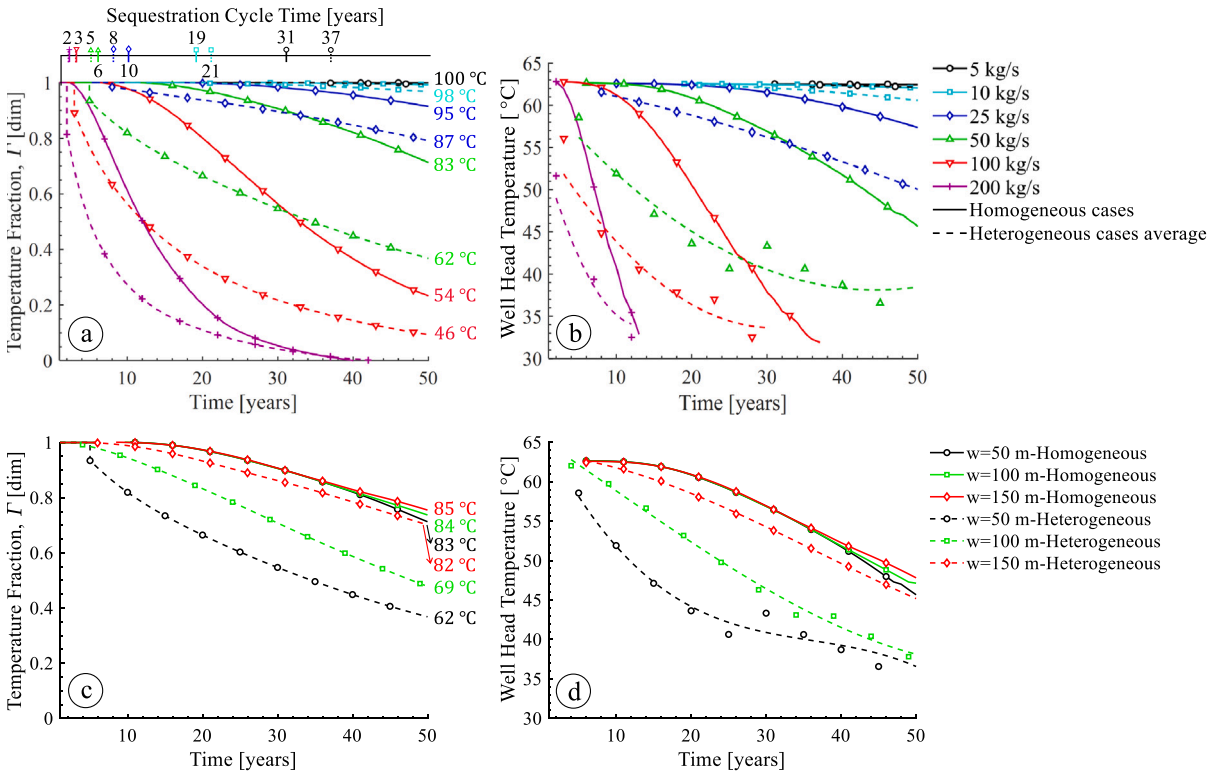

Fig. 6. Production well temperature fraction (Γ) and production wellhead temperature versus flowrate for constant channels' width $w = 50$ m (a & b), and versus channels' width for constant injection rate $\dot{m}_{inj} = 50$ kg/s (c & d). These plots also indicate the sequestration time and CPG lifetime, as well as the aquifer thermal depletion for different cases.

words, the heterogeneous case becomes similar to its representative homogeneous case. Secondly, the temperature drop is less in aquifers with higher channels' width (higher average porosity and permeability) compared to lower w case. For instance, for the injection rate of 50 kg/s, the temperature drop over 50 years for the cases with w = 100 m and w = 150 m is about 18% and 53% lower compared to the w = 50 m case, respectively. This is because as w increases, not only does the average pore volume (flow cross-section area) increase but also channels' vertical connection increases, and the permeability in the y–direction (k_y) is improved. Therefore, for a constant mass flowrate, the CO_2 flooding front moves slower horizontally, and the upward movement of $scCO_2$ due to the buoyancy effect becomes easier and the CO_2 travel in upper levels of the aquifer intensifies. As a result, $scCO_2$ vertical flow increases despite the uniform and piston-like movement in lower channels' widths (Fig. 7), and the $scCO_2$ *thermal plume* reaches the production well at a later time compared to lower w cases; subsequently, thermal depletion decreases.

Fig. 8 shows the values of $scCO_2$ production rate and inverse mobility (M), calculated every time step. From Fig. 8a and c, it is observed that heterogeneity has a negligible effect on the CO_2 production rate. Also, the CO_2 production rates are slightly lower than their injection rates. This indicates there are some CO_2 loss in the reservoir, and that not all the injected CO_2 reaches the production well. This loss is more sensible for lower injection rates and impairs the CPG performance by reducing the production mass flowrate. While the effect of heterogeneity on the production rate is negligible, heterogeneity increases the aquifer pressure drop in heterogeneous cases. It results in higher inverse mobility (M) values compared to their homogeneous cases by about 1.2, 1.5, and 1.7 times for cases with w = 150, 100, and 50 m, respectively (Fig. 8d). The value of M (which is essentially the aquifer impedance), becomes relatively constant after about 5 years for high injection rates (100 and 200 kg/s) and after about 10 years for lower injection rates (Fig. 8b). Also, M is considerably higher for a brine-geothermal system, and therefore, the thermosiphon performance of CO_2 is significantly higher than that of brine, especially in shallow aquifers [17].

Fig. 9a shows the values of the CPG cycle excess pressure (P_{excess}) for different injection rates. Ideally, when thermal depletion happens at a very slow pace, such as in the cases with 5 kg/s and 10 kg/s flowrates, the maximum P_{excess} (about 5.4 MPa) is achieved at the surface power plant. However, as observed from the results of the temperature fracture (Fig. 6a), the aquifer gradually thermally depletes as CO_2 is injected. By decrease in the downhole temperature of the production well, the CO_2 density gradient between the two wells decreases and consequently, the thermosiphon is weakened. For high injection rates, P_{excess} decreases faster and therefore, the CPG lifetime will be shorter. For the homogeneous cases that represent the aquifer with $w = 50$ m (k_{avg} = 225.5 mD), the CPG power plant operation time (the span between the sequestration stage and CPG lifetime) is about 19, 31, 40, 44, 34, and 11 years for the injection rates of 5, 10, 25, 50, 100, and 200 kg/s, respectively. Therefore, it is observed that the case with an injection rate of 50 kg/s provides the highest CPG operation time.

Although heterogeneity slightly affects the CPG lifetime, it has a significant impact on P_{excess} (Fig. 9b). In an aquifer with the presence of fluvial channels, the average value of P_{excess} that thermosiphon provides is about 34%, 20%, and 5% lower for cases with w = 50 m, 100 m, and 150 m, respectively, compared with their representative homogeneous cases.

The instantaneous net electric power generation values, from the sequestration stage to the CPG lifetime, are found for each aquifer realization (Fig. 2) and are displayed in Fig. 10(a) with fixed channels' width (w = 50 m), and in Fig. 10(b) with fixed injection rate ($\dot{m}_{inj}$ = 50 kg/s). During the initial years of injection, the net power is ascending. This is because, at the initial stage, the $scCO_2$ production rate is increasing, the inverse mobility M is decreasing, and the thermal plume has not yet reached production well. Therefore, a maximum point happens after the PE stage, resulted from the interactions between the aquifer mobility and temperature drop at the production well.

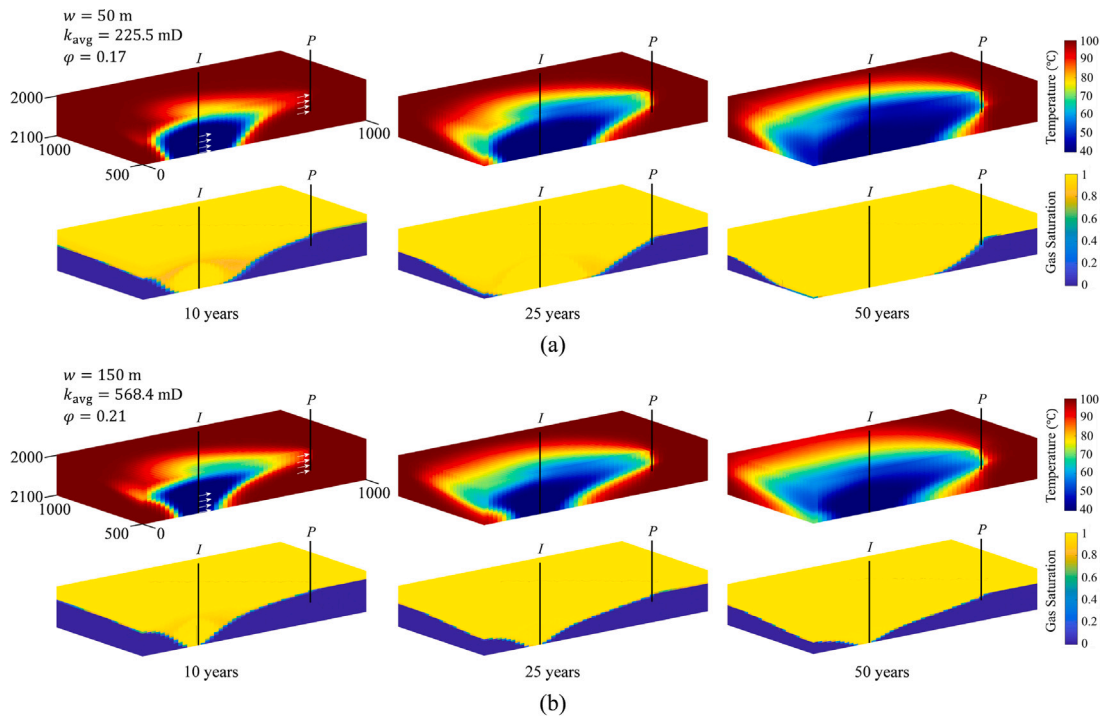

Fig. 7. Temperature and gas saturation distribution at different time-steps for homogeneous cases, representing (a) $w = 50$ m and (b) $w = 150$ m, and injection rate of $\dot{m}_{inj} = 50$ kg/s. As k_{avg} increases, k_y increases as well; and CO_2 disperses more vertically and reaches the production well in a later time.

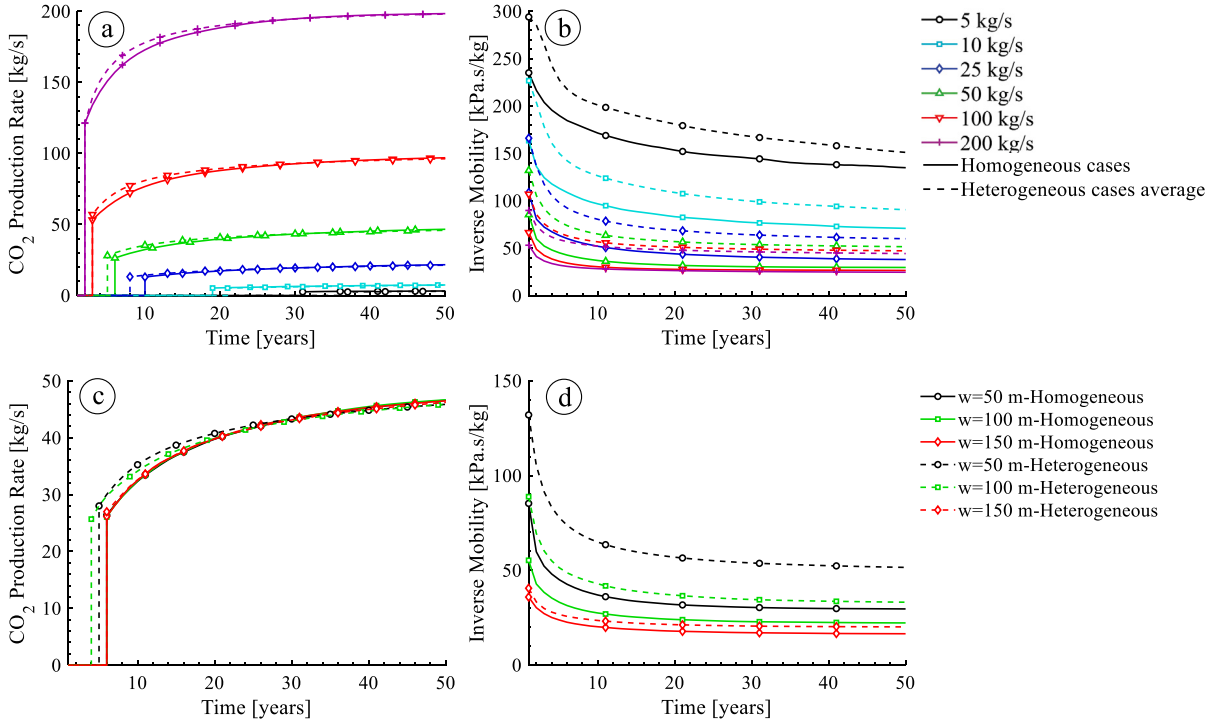

Fig. 8. CO_2 production rate and the aquifer impedance (inverse mobility) versus flowrate for constant channels' width $w = 50$ m (a & b), and versus channels' width for constant injection rate $\dot{m}_{inj} = 50$ kg/s (c & d).

After this point, when the CO_2 thermal plume reaches the production well, aquifer thermal depletion occurs and the temperature fraction (Γ) decreases, resulting in a decrease in net power. As the injection rate is increased, contrary to the CPG cycle lifetime, the maximum value of net power increases. For the homogeneous case with $\dot{m}_{inj} = 200$ kg/s, the maximum net power is about 1.34 MW_e. Nevertheless, this value decreases to about 0.82 MW_e for the representative heterogeneous case. Again, it is observed that fluvial heterogeneity, especially with lower channels' width (50 m), significantly decreases the instantaneous net power. Therefore, considering a homogeneous aquifer for CPG representation can overestimate the net power output to about 3 times the actual heterogeneous reservoir.

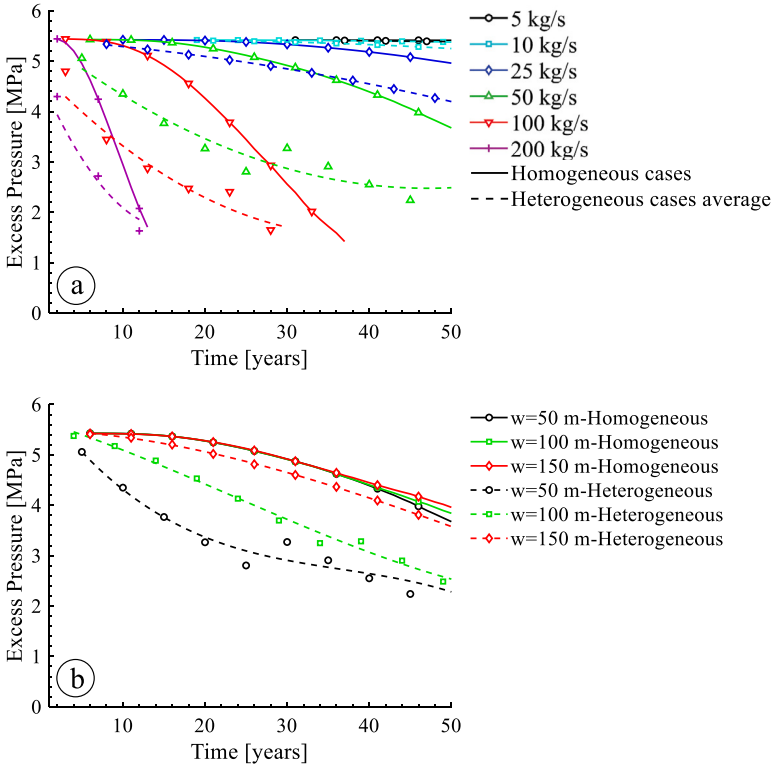

Fig. 9. CPG cycle excess pressure for (a) different flowrates and constant channels' width $w = 50$ m, and (b) for different channels' width and constant injection rate $\dot{m}_{inj} = 50$ kg/s.

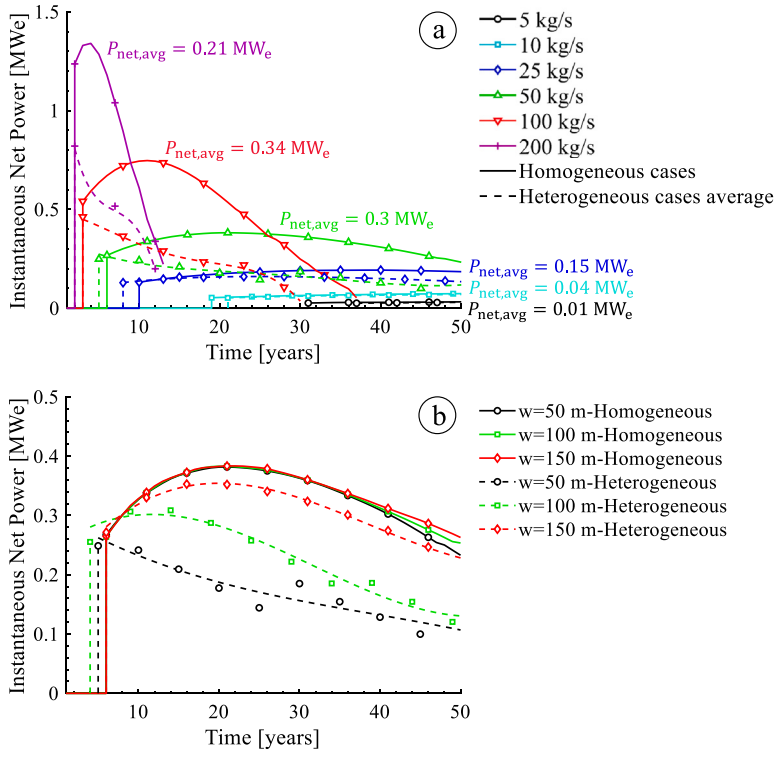

Fig. 10. Instantaneous net power for (a) different flowrates and constant channels' width $w = 50$ m, and (b) for different channels' width and constant injection rate $\dot{m}_{inj} = 50$ kg/s. $P_{net,avg}$ shows the average produced net power over 50 years.

The CPG system's cumulative net power over 50 years, from the sequestration stage to the CPG lifetime, is illustrated in Fig. 11(a). Since we observed that the injection rate has a significant effect on both the sequestration stage and the CPG lifetime, it is vital to find an optimum injection rate that observes a balance between these two periods and provides the highest output power. It was concluded in the previous sections that the injection rate of 50 kg/s provides the longest CPG cycle operation time (44 years), over the 50 years of injection. From

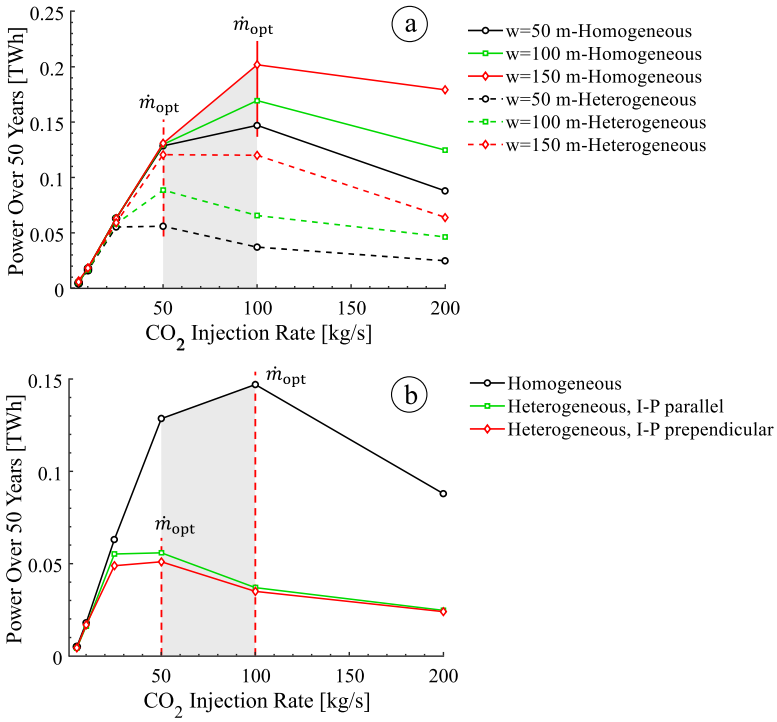

Fig. 11. Cumulative power over 50 years for different channels' width and heterogeneity cases.

Fig. 11(a), the optimum injection rate for the homogeneous cases of the present paper is about 100 kg/s and for the heterogeneous cases is about 50 kg/s. Heterogeneous cases have a lower optimum injection rate because thermal depletion and temperature drop happen faster in these cases. Additionally, heterogeneity has reduced the CPG system cumulative power over 50 years by about 75%, 61%, and 41% for w = 50, 100, and 150 m, respectively, for the 100 kg/s cases. Meanwhile, for lower injection rates ($\dot{m}_{inj}$ < 10 kg/s) heterogeneity has a negligible effect on the cumulative net power and therefore, can be overlooked. The grey area in Fig. 11, shows the region where the optimum injection rate happens.

It is expected that the I-P line orientation with respect to the channels' orientation affects the pressure drop, CO_2 and temperature distribution in the aquifer. Therefore the overall CPG performance is affected. We previously studied doublet well patterns and it was observed that the I-P line parallel to channels provides the highest performance [22,59]. In the present study, effects of I-P line orientation in heterogeneous cases with a single injection-production well pair are analysed. Fig. 11(b) shows the overall CPG performance for aquifers without channels, with I-P line parallel to channels, and with I-P line perpendicular to channels' orientation. In cases with parallel I-P line, the thermal plume extension toward the production well is almost the same as the perpendicular cases. However, the CO_2 thermal plume mostly expands in the direction of channels and therefore, it sooner reaches the production well. Thus, thermal depletion happens faster in parallel cases (Fig. 12). Similarly for the CO_2 saturation in parallel cases – in a similar time-frame with the perpendicular ones – the CO_2 saturation near the production well is much higher. In contrast, in the perpendicular cases, channels misdirect CO_2 propagation and prevent it from reaching the production well. This results in considerably shorter sequestration times and more importantly, higher CO_2 production rates for parallel cases. Resulting from a combination of factors such as faster thermal depletion, lower sequestration time, higher CO_2 saturations and flowrates, and lower pressure drop, it is observed that the cases with I-P line parallel to the channels' orientation provide a higher cumulative power generation by about 10% compared to the perpendicular cases (Fig. 11(b)).

3.2. Adjusting flowrate and constant excess pressure

As observed in Section 3.1, due to the aquifer thermal depletion, the CPG performance is dropped and at some point (when either the CO_2 temperature or pressure falls below the critical values) the system is stopped to prevent possible damage to the turbine. Therefore, it is important to constantly have a supercritical fluid at the turbine's inlet. As a result, a lower bound for P_{excess} (3.5 MPa) is defined, and by adjusting the system flowrate, we keep the system above the operational limit. Initially, CO_2 is injected at the rate of 50 kg/s, and when the PE stage has passed, the flowrate is updated on a yearly basis. The optimum flowrate is a result of the balance between the P_{excess}, aquifer pressure loss, and temperature drop. The injection and the production rates for the homogeneous cases are shown in Fig. 13. At some point, to observe the $P_{excess} \geq 3.5$ MPa condition, the injection rate moves toward zero, which defines the power cycle lifetime. The CPG operation time is about 45, 34, and 23 years for the homogeneous cases of k_{avg} = 225.5, 336.5, and 568.5 mD, respectively.

Fig. 14 shows the production well bottomhole temperature, wellhead temperature, excess pressure, and the cumulative power over 50 years, for the cases with adjusting CO_2 injection rate. The adjusting injection rate almost obeys the lower bound that is considered for P_{excess} (3.5 MPa), and it is observed that for only a few time steps, P_{excess} falls below the limit. This is because the injection rate is updated yearly and that the system has a response time, meaning that it takes some time for the updated injection rate to have its impact on the production well temperature. The considered bound for P_{excess} also results in lower bounds for the well bottomhole temperature (80 °C) and for the wellhead temperature (42.5 °C) as well. This means that we can rely on the CPG system to produce $scCO_2$ with the minimum surface temperature of 42.5 °C and the pressure of at least 9.5 MPa ($P_1 + P_{excess}$ from Fig. 5) during the CPG lifetime.

From Fig. 14a, b, and c, the CPG system in a heterogeneous aquifer has a shorter response time and is controlled better. However, from Fig. 14d, we see that the cumulative electric power is about 70%, 50%, and 18% lower for the heterogeneous cases of w = 50, 100, and 150 m, compared to their representative homogeneous cases.

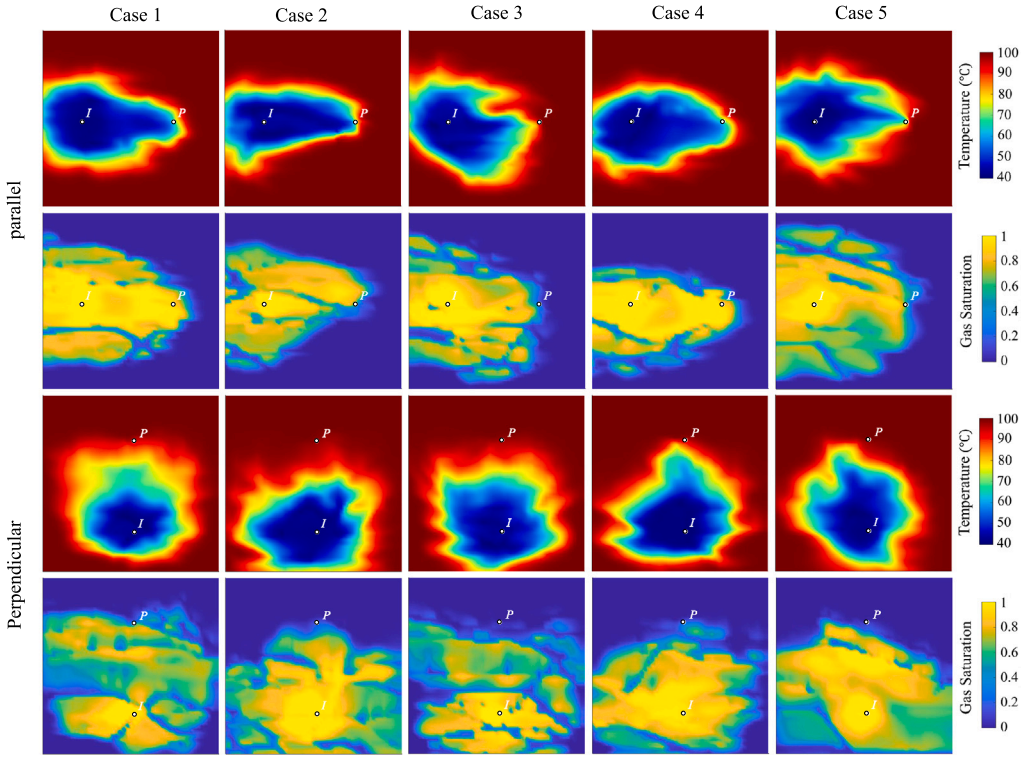

Fig. 12. Temperature and CO_2 saturation distribution at the mid-surface of the reservoir (2050 m) for the parallel and perpendicular heterogeneous cases with channels' width of $w = 50$ m after 25 years of injection.

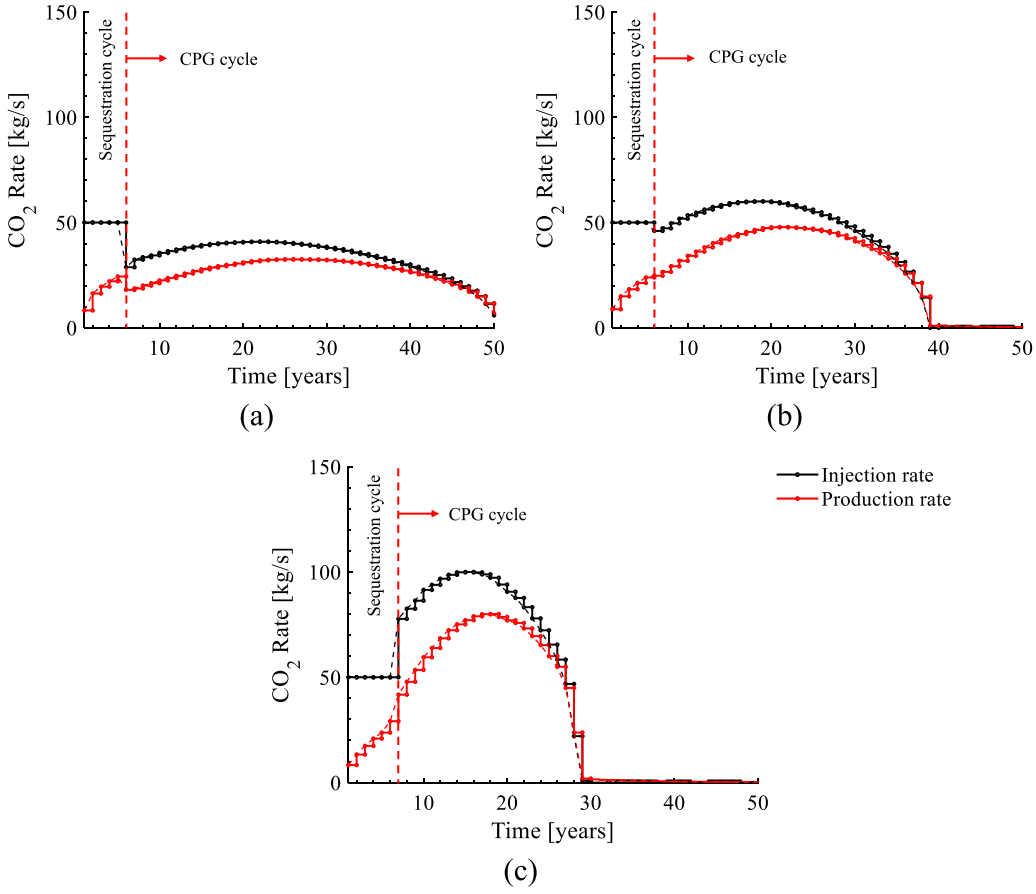

Fig. 13. Optimized CO_2 injection rate and the resulted production rate for the homogeneous cases of (a) $k_{avg} = 225.5$ mD or $w = 50$ m, (b) $k_{avg} = 336.5$ mD or $w = 100$ m, and (c) $k_{avg} = 568.5$ mD or $w = 150$ m.

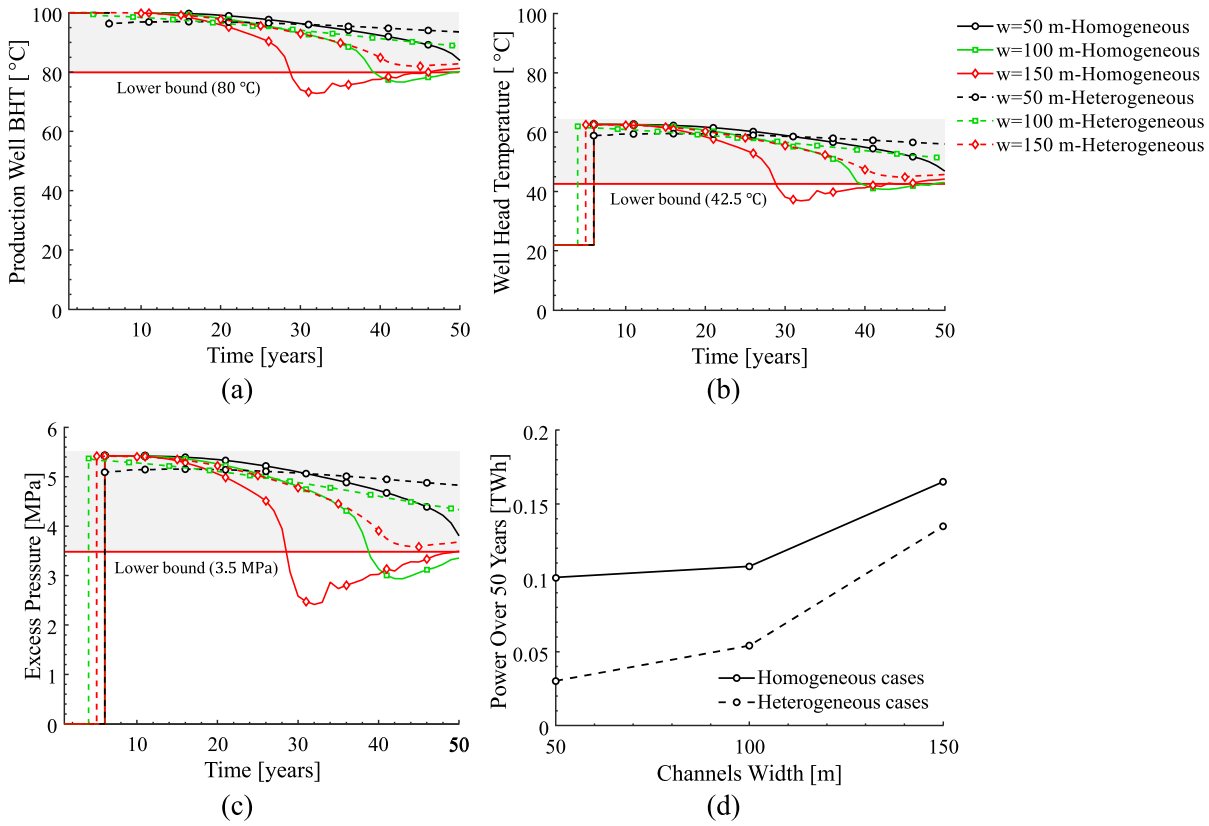

Fig. 14. Optimized CO_2 injection rate results: (a) production well bottomhole temperature, (b) production wellhead temperature, (c) CPG cycle excess pressure, and (d) cumulative power over 50 years for different channels' width and heterogeneity cases.

4. Conclusions and remarks

Performance and electric power generation and limits of a direct-CO_2 thermosiphon system combined with a CO_2 expansion turbine cycle in both homogeneous and 3D fluvial braided heterogeneous aquifers, with different channels' widths, are studied in this paper.

The key findings can be summarized as below:

- The CO_2 injection rate considerably affects the required sequestration stage for CO_2 to reach a minimum pore-space saturation of about 0.3. As a result, flowrates such as 5 and 10 kg/s that have a very long CO_2-plume establishment stage (about 20 to 35 years) are not applicable for a single pair of wells.
- The aquifer thermal depletion and the production temperature drop are two of the main problems affecting the thermosiphon. Additionally, fluvial heterogeneity deteriorates thermal depletion by a value between 22% and 120%, depending on the channels' width.
- Since the produced CO_2 is directly used in an expansion turbine, it is important that CO_2 is produced at its supercritical phase in the production well. The time that CO_2 falls below the supercritical condition defines the cycle lifetime. Higher injection rates have a shorter cycle lifetime due to their faster aquifer thermal depletion (as expected).
- The I-P line orientation with respect to channels affects both CO_2 and thermal plume distributions inside the aquifer. Cases with the I-P line parallel to the channels' orientation provide higher cumulative power by 10% compared to the cases with I-P perpendicular to channels.
- Among the considered injection rates, $\dot{m}_{inj}$ = 50 kg/s provided the highest CPG cycle operation time by about 44 years (the span between the sequestration stage and the CPG lifetime).
- CO_2 injection rate of 100 kg/s provides the highest performance in homogeneous cases, considered in the present study, with cumulative power generation of about 0.15, 0.17, and 0.20 TWh for k_{avg} = 225.5, 336.5, and 568.5 mD, respectively. On the other hand, the injection rate of 50 kg/s is the optimum rate in heterogeneous cases of the present study and provides about 0.06, 0.09, and 0.12 TWh for w = 50, 100, and 150 m, respectively. To put this in perspective, according to [65], a typical domestic household in the UK consumes about 258 kWh per month. Therefore, should the CPG described in the present study work in its optimal performance ($\dot{m}_{inj}$ = 100 and 50 kg/s for homogeneous and heterogeneous aquifers, respectively), it can provide the required electricity for about 1500 households[1] over 43 years lifetime and 860 households over 45 years lifetime for the CPG working in homogeneous and heterogeneous aquifers with w = 150 m, respectively.
- Neglecting the heterogeneous nature of aquifers can result in an overestimation both in cycle electric power output and lifetime. The presence of fluvial heterogeneity in the aquifer decreases the CPG performance up to about 75%, depending on the channels' width and CO_2 injection rate.

Results suggest that for a CPG system, to provide acceptable electric power and to become commercial, high mass flowrates are required (50 to 100 kg/s). However, these values for injection rate are relatively high to be practical for a single injection/production well pair. For example in Sleipner, the injection rate of the single injection well is 1 million tonne per year of CO_2 which is around 32 kg/s [66]. Or in Cranfield Geological Carbon Sequestration Project, the maximum injection rate per well is only 500 kg/min or 8.33 kg/s [67,68]. Or

[1] (0.2 TWh/43 years)/(285 kWh/month).

in the North Sea, median UK oil and gas production rate corresponds to around 0.35 Mt/yr/well or 11.1 kg/s/well of CO_2 [69]. Therefore, to inject 50 kg/s, several injection and production wells are required. In this scenario, well patterns [23] and perforation cost are two major issues. In addition, by dividing the injection rate into smaller values, the sequestration stage increases, which is not desirable. To tackle these issues, two alternative scenarios are proposed. The first is to use CPG in depleted oil reservoirs, or the reservoirs that currently include CO_2 from sequestration processes, such as the SECARB Cranfield Site that a brine-saturated sand has been under CO_2 flood [14]. The second is to use CPG in shallower depths and smaller scales for peak shaving purposes, such as [70,71]. In the latter approach, when the cost of energy is low, CO_2 is injected into the reservoir but the production well is shut down, letting the CO_2 to warm-up and reach the required mass-fraction at the production well; and when the cost of energy is high, $scCO_2$ production starts and cheap renewable geothermal electricity substitutes the expensive fossil fuel-based one. In the peak shaving approach, the reservoir is used as on-site energy storage, and since energy is produced in discrete periods, time is given to the reservoir to recover its temperature and compensate for the thermal depletion.

Another remark is about the electricity output of CPG that we found to be in order of tenth of TWh. This value is small, however, we need to consider expanding CPG across multiple wells and deeper, hotter systems. Additionally, one must consider the value of CCS and CCUS, that is, both sequestering CO_2 at the end of operation, and utilizing CO_2 for the operation. The calculation of revenue from CCS and CCUS is not straightforward. However, an analysis by the Committee on Climate Change [72] in 2018 indicates that CCUS will be the only way to decarbonize certain key industrial sectors before 2050. They recommend that 10 MtCO2 should be stored annually by 2030, 3 MtCO2 of which are from industry, to maintain the option of high levels of deployment by 2050, potentially over 100 MtCO2/year. CPG will be an attractive CCUS option to practice the engineering of large volume of CO_2 storage needed beyond 2050. Assuming 50 kg/s of CO_2 injection, a CPG operation can utilize 1.58 MtCO2/year that will be stored at the end of operation.

The results and the discussion about the merits and demerits of CPG in this paper can provide guidelines for possible future works to enhance and optimize the CPG technology. Also, this paper proposed a method to prevent possible power over-predictions that are resulted from field uncertainties.

CRediT authorship contribution statement

Amir Mohammad Norouzi: Conceptualization, Methodology, Software, Investigation, Formal analysis, Writing – original draft, Writing – review & editing. **Fatemeh Pouranian:** Software, Methodology. **Arash Rabbani:** Software, Methodology. **Neil Fowler:** Conceptualization. **Jon Gluyas:** Conceptualization, Writing – review & editing. **Vahid Niasar:** Conceptualization, Writing – review & editing. **Justin Ezekiel:** Conceptualization, Writing – review & editing. **Masoud Babaei:** Conceptualization, Methodology, Supervision, Project administration, Writing – review & editing.

Declaration of competing interest

The authors declare that they have no known competing financial interests or personal relationships that could have appeared to influence the work reported in this paper.

Data availability

Data will be made available on request.

Acknowledgement

The authors acknowledge the University of Manchester President's Doctoral Scholar (PDS) award to Amir Mohammad Norouzi that made this research possible.

Appendix. Parameters sensitivity analysis

In this section, the effects of three sets of parameters, including geochemical reactions, bottomhole temperature of the injected CO_2, and channels' porosity and permeability, on the system performance and power output are considered. The base case for the sensitivity analysis is a heterogeneous aquifer with a channel width of 50 m, a porosity of 0.25, a permeability of 1000 mD, and an injection rate of 50 kg/s.

A.1. Geochemical reactions and salt precipitation

Geochemical reactions, specifically salt precipitation, can affect the aquifer injectivity and, therefore, the overall power output of the CPG system. However, it was shown that the dominant precipitation is due to water vaporization and salt precipitation near the injection well [21,50]. The aquifer considered to study the effects of geochemical reactions is a heterogeneous high-salinity sandstone aquifer with a salinity of 15% by weight, channels' thickness of $w = 50$ m, and $k_{avg} = 250$ mD. Carbonate, silicate, and clay minerals, including calcite, anorthite, and kaolinite are among the most common components of such aquifers. To study the effects of geochemical reactions, both aqueous and mineral reactions are considered based on previous works by Norouzi et al. [21],Nghiem et al. [73], and Cui et al. [19]. Complete details of these reactions, including reactions' equilibrium coefficients and minerals' rate law equation parameters are provided in Appendix A of the work by Norouzi et al. [21].

$$H^+ + OH^- \rightleftharpoons H_2O \tag{A.1a}$$

$$CO_2 + H_2O \rightleftharpoons HCO_3^- + H^+ \tag{A.1b}$$

$$HCO_3^- \rightleftharpoons CO_3^{2-} + H^+ \tag{A.1c}$$

$$\text{Calcite} + H^+ \rightleftharpoons Ca^{2+} + HCO_3^- \tag{A.1d}$$

$$\text{Anorthite} + 8H^+ \rightleftharpoons 4H_2O + Ca^{2+} + 2Al^{3+} + 2SiO_{2,aq} \tag{A.1e}$$

$$\text{Kaolinite} + 6H^+ \rightleftharpoons 5H_2O + 2Al^{3+} + 2SiO_{2,aq} \tag{A.1f}$$

$$\text{Halite} \rightleftharpoons Na^+ + Cl^- \tag{A.1g}$$

The initial composition of the brine and the aquifer are presented in Table A.2.

Here, two scenarios are considered. First, we consider the heterogeneous cases that include CO_2 and brine, but no geochemical reaction happens between them, and second, we consider the same cases with geochemical reactions occurring in the aquifer. The results are shown in Fig. A.1. Fig. A.1a shows the amount of the precipitated salt resulting from water vaporization. In agreement with the findings of previous works, such as [21,50], salt is the main mineral that precipitates and affects aquifer injectivity. Salt precipitation mainly happens in the dry-out region close to the injection well and therefore reduces the injectivity in this area. From Fig. A.1b it is observed that the precipitated

Table A.2
Aquifer and brine initial compositions.

Brine	Ion	H^+	Ca^{2+}	Al^{3+}	$SiO_{2,aq}$	Na^+	Cl^-
	mol.L^{-1}	1×10^{-7}	9.12×10^{-5}	2.32×10^{-11}	2.35×10^{-8}	1	1
	Ion	HCO_3^-	CO_3^{2-}	OH^-			
	mol.L^{-1}	2.5×10^{-2}	1.2×10^{-5}	5.45×10^{-7}			
Mineral	Component		Anorthite	Calcite	Kaolinite	Halite	
	Volume fraction		0.036	0.153	0.00135	0.00	

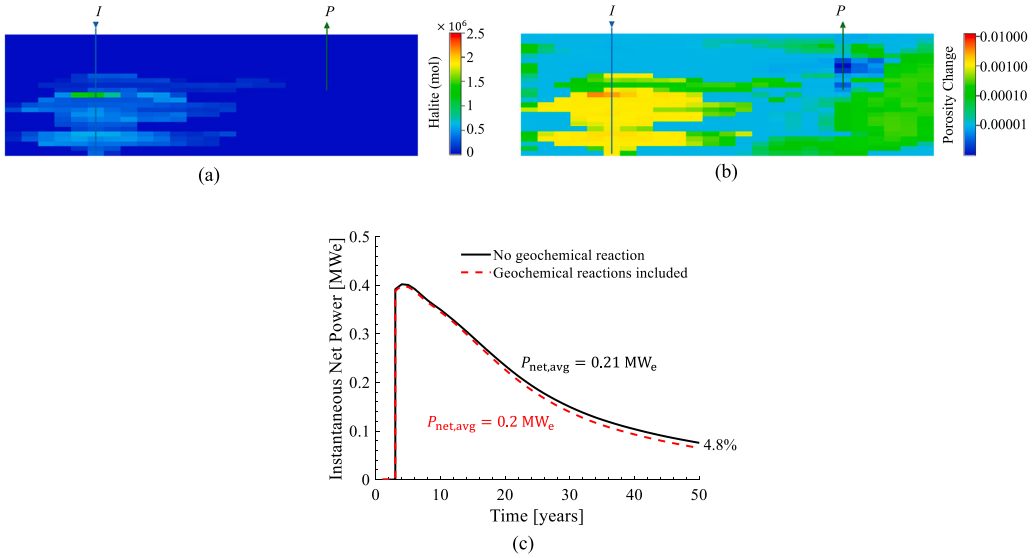

Fig. A.1. Geochemical reactions sensitivity analysis: (a) salt precipitation resulting from water vaporization in the dry-out region near the injection well after 50 years of injection, (b) variations in aquifer's porosity due to minerals' precipitation and dissolution after 50 years, and (c) the effect of geochemical reactions on the instantaneous power output of the system versus time.

salt near the injection well can reduce the aquifer porosity up to 0.01, which is about a 4% reduction in porosity near the injection well. Also, it is observed that far from the injection well, the aquifer porosity is slightly increased, which is mainly due to minerals' dissolution into water. Fig. A.1c shows the instantaneous net power of the system for the cases with and without geochemical reactions. Geochemical reactions mainly affect the injectivity and therefore, pressure build-up near the injection well and CO_2 flow and distribution. However, in cases considered for the present study, since the injection mass flowrate is kept constant, the CO_2 and temperature distribution remain the same and only the pressure build-up at the injection well increases. An increase in the injection well bottomhole pressure will lead to an increase in injection wellhead pressure, *i.e.*, the required injection pressure increases. The increase in the required pumping pressure, will reduce the amount of the excess pressure achieved from the surface, and therefore, reduces the system's output power. However, the scale of the reduction in excess pressure is small, and the average reduction in the CPG output power is about 4.8%.

A.2. CO_2 bottomhole injection temperature

One of the parameters that can affect the temperature distribution, and consequently the system's performance, is the CO_2 injection temperature. CO_2 injection temperature is defined from the injection head temperature and the isentropic (adiabatic and reversible) compression process that occurs by reaching the aquifer depth. As a result, to increase the CO_2 injection temperature, higher temperature and pressure at the surface are required, meaning that the enthalpy gradient between the injection and production streams decreases and subsequently the system power production decreases as well.

Fig. A.2a shows the temperature distribution in the aquifer for three different CO_2 injection temperatures. As the injection temperature increases, the temperature distribution becomes more uniform, and the temperature depletion rate decreases. This results in slightly higher bottomhole temperature at the production well, for instance, after 50 years, the production bottomhole temperature will be 72.9, 76.7, and 80.4 °C for the cases with injection temperatures of 40, 50, and 60 °C, respectively. Despite this increase in production bottomhole temperature, since the enthalpy gradient becomes smaller for cases with higher injection temperature, it is found that as the injection temperature increases, the average net power decreases (Fig. A.2b).

A.3. Channels' porosity and permeability

To study the effects of channels' porosity and permeability three sets of heterogeneous aquifers are considered as follows: (i) $\phi = 0.25$, $k = 1000$ mD, and $k_{avg} = 250$ mD, (ii) $\phi = 0.23$, $k = 800$ mD, and $k_{avg} = 203$ mD, and (iii) $\phi = 0.21$, $k = 600$ mD, and $k_{avg} = 157$ mD.

Fig. A.3 shows the CPG instantaneous net power for cases with different channels' permeability and porosity. Since the injection rate is kept constant at the rate of 50 kg/s, the CO_2-plume and the temperature distribution in the aquifer are almost the same for all these cases. However, as the aquifer transmissibility decreases, a higher parasitic pressure drop happens, resulting in lower excess pressure at the surface and consequently lower system output power. It is observed that a reduction of about 37% in the aquifer's average permeability results in a 7% reduction in output net power from 0.28 to 0.26 MW$_e$. Also, it is observed that as time goes on, the decrease in instantaneous net power increases. This is because CO_2 gradually disperses in the aquifer and as it reaches different layers of the aquifer, more pressure drop due to lower permeability and porosity occurs and therefore, the net power decreases more.

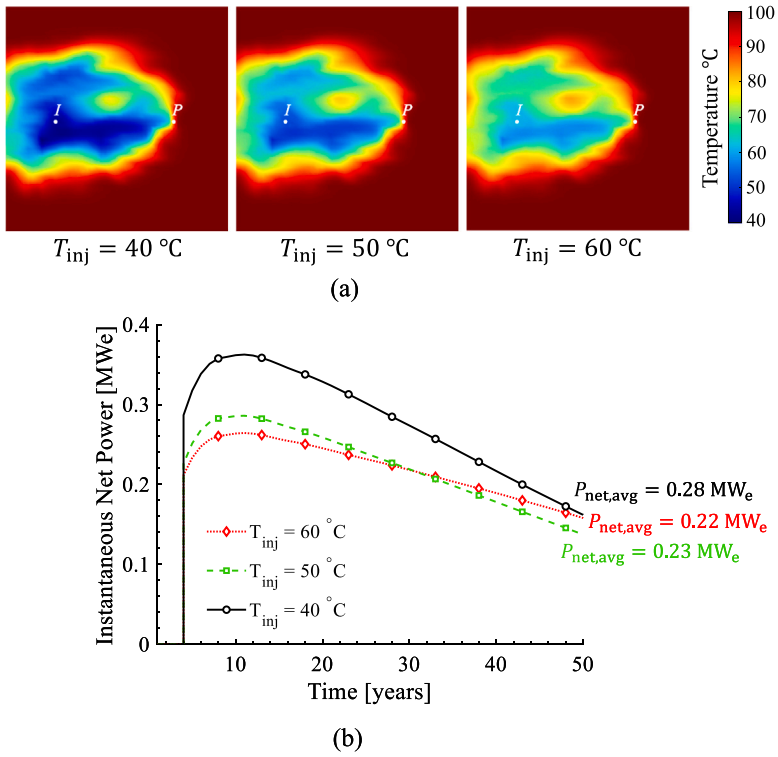

Fig. A.2. CO_2 bottomhole injection temperature sensitivity analysis: (a) temperature distribution at the mid-surface of the aquifer (2050 m) after 25 years of injection, and (b) instantaneous net power versus time.

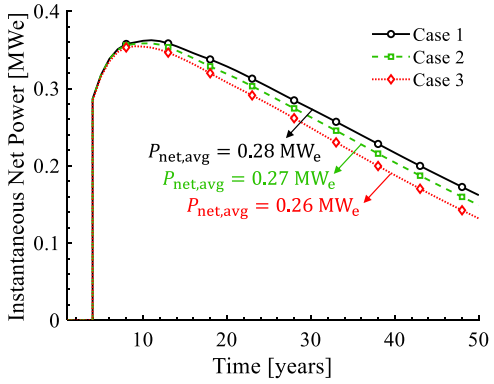

Fig. A.3. Effects of channels' porosity and permeability on the overall system performance and the instantaneous net power versus time.

Nomenclature

A	Cross-sectional area, [m^2]
h	Specific enthalpy, [J kg^{-1}]
k	Permeability, [mD, m^2]
L	Length, [m]
$\dot{m}$	Mass flowrate, [kg s^{-1}]
P	Pressure, [Pa, MPa]
P_{net}	Net power, [MW_e, TWh]
Q	Mass vapour quality, [–]
s	Specific entropy, [J kg^{-1} $°C^{-1}$]
T	Temperature/channels' thickness, [°C, m]
t	Time, [year]
w	Channels' width, [m]
X_{CO_2}	CO_2 mass-fraction in gas phase, [–]
Γ	Temperature fraction, [–]
η	Efficiency, [–]
λ	Parasitic load fraction [–]
μ	Viscosity, [Pa s]
ρ	Density, [kg m^{-3}]
ϕ	Porosity, [–]

References

[1] International Energy Agency (IEA). CO2 emissions from fuel combustion 2019 edition. 2019, URL https://iea.blob.core.windows.net/assets/eb3b2e8d-28e0-47fd-a8ba-160f7ed42bc3/CO2_Emissions_from_Fuel_Combustion_2019_Highlights.pdf.

[2] Sayigh A. Renewable energy — the way forward. Appl Energy 1999;64(1):15–30.

[3] Abas N, Khan N. Carbon conundrum, climate change, CO2 capture and consumptions. J CO2 Util 2014;8:39–48.

[4] Metz B, on Climate Change IP, on Climate Change. Working Group III. IP, d'experts intergouvernemental sur l'évolution du climat. Working Group III G, on Climate Change Working Group Technical Unit IP, Intergovernmental Panel on Climate Change. Working Group 3 P, et al. Carbon dioxide capture and storage: Special report of the intergovernmental panel on climate change. 25 CM, Cambridge University Press; 2005.

[5] Farajzadeh R, Eftekhari A, Dafnomilis G, Lake L, Bruining J. On the sustainability of CO2 storage through CO2 – enhanced oil recovery. Appl Energy 2020;261:114467.

[6] Rezk MG, Foroozesh J. Determination of mass transfer parameters and swelling factor of CO2-oil systems at high pressures. Int J Heat Mass Transfer 2018;126:380–90.

[7] Babaei M, Mu J, Masters AJ. Impact of variation in multicomponent diffusion coefficients and salinity in CO2-EOR: A numerical study using molecular dynamics simulation. J Pet Sci Eng 2018;162:685–96.

[8] Mohagheghian E, Hassanzadeh H, Chen Z. CO2 sequestration coupled with enhanced gas recovery in shale gas reservoirs. J CO2 Util 2019;34:646–55.

[9] Ezekiel J, Ebigbo A, Adams BM, Saar MO. Combining natural gas recovery and CO2-based geothermal energy extraction for electric power generation. Appl Energy 2020;269:115012.

[10] Pruess K. Enhanced geothermal systems (EGS) using CO2 as working fluid—A novel approach for generating renewable energy with simultaneous sequestration of carbon. Geothermics 2006;35(4):351–67.

[11] Brown D. A hot dry rock geothermal energy concept utilizing supercritical CO2 instead of water. In: Proceedings of the twenty-fifth workshop on geothermal reservoir engineering. 2000.

[12] Wang C-L, Cheng W-L, Nian Y-L, Yang L, Han B-B, Liu M-H. Simulation of heat extraction from CO2-based enhanced geothermal systems considering CO2 sequestration. Energy 2018;142:157–67.
[13] Randolph JB, Saar MO. Combining geothermal energy capture with geologic carbon dioxide sequestration. Geophys Res Lett 2011;38(10).
[14] Pan L, Doughty C, Freifeld B. How to sustain a CO2-thermosiphon in a partially saturated geothermal reservoir: Lessons learned from field experiment and numerical modeling. Geothermics 2018;71:274–93.
[15] Adams BM, Vogler D, Kuehn TH, Bielicki JM, Garapati N, Saar MO. Heat depletion in sedimentary basins and its effect on the design and electric power output of CO2 plume geothermal (CPG) systems. Renew Energy 2021;172:1393–403.
[16] Garapati N, Adams BM, Fleming MR, Kuehn TH, Saar MO. Combining brine or CO2 geothermal preheating with low-temperature waste heat: A higher-efficiency hybrid geothermal power system. J CO2 Util 2020;42:101323.
[17] Adams BM, Kuehn TH, Bielicki JM, Randolph JB, Saar MO. On the importance of the thermosiphon effect in CPG (CO2 plume geothermal) power systems. Energy 2014;69:409–18.
[18] Buscheck TA, Bielicki JM, Edmunds TA, Hao Y, Sun Y, Randolph JB, et al. Multifluid geo-energy systems: Using geologic CO2 storage for geothermal energy production and grid-scale energy storage in sedimentary basins. Geosphere 2016;12(3):678–96.
[19] Cui G, Zhang L, Tan C, Ren S, Zhuang Y, Enechukwu C. Injection of supercritical CO2 for geothermal exploitation from sandstone and carbonate reservoirs: CO2–water–rock interactions and their effects. J CO2 Util 2017;20:113–28.
[20] Cui G, Ren S, Rui Z, Ezekiel J, Zhang L, Wang H. The influence of complicated fluid-rock interactions on the geothermal exploitation in the CO2 plume geothermal system. Appl Energy 2018;227:49–63.
[21] Norouzi AM, Babaei M, Han WS, Kim K-Y, Niasar V. CO2-plume geothermal processes: A parametric study of salt precipitation influenced by capillary-driven backflow. Chem Eng J 2021;130031.
[22] Norouzi AM, Gluyas J, Babaei M. CO2-plume geothermal in fluvial formations: A 2D numerical performance study using subsurface metrics and upscaling. Geothermics 2022;99:102287.
[23] Babaei M. Integrated carbon sequestration–geothermal heat recovery: Performance comparison between open and close systems. Transp Porous Media 2019;126(1):249–73.
[24] Schifflechner C, Wieland C, Spliethoff H. CO2 plume geothermal (CPG) systems for combined heat and power production: An evaluation of various plant configurations. J Therm Sci 2022.
[25] Schifflechner C, Dawo F, Eyerer S, Wieland C, Spliethoff H. Thermodynamic comparison of direct supercritical CO2 and indirect brine-ORC concepts for geothermal combined heat and power generation. Renew Energy 2020;161:1292–302.
[26] Ezekiel J, Adams BM, Saar MO, Ebigbo A. Numerical analysis and optimization of the performance of CO2-plume geothermal (CPG) production wells and implications for electric power generation. Geothermics 2022;98:102270.
[27] Fleming MR, Adams BM, Kuehn TH, Bielicki JM, Saar MO. Increased power generation due to exothermic water exsolution in CO2 plume geothermal (CPG) power plants. Geothermics 2020;88:101865.
[28] Allen PA, Allen JR. Basin analysis: principles and application to petroleum play assessment. John Wiley & Sons; 2013.
[29] Einsele G. Sedimentary basins: evolution, facies, and sediment budget. Springer Science & Business Media; 2000.
[30] Hartmann J, Moosdorf N. The new global lithological map database GLiM: A representation of rock properties at the earth surface. Geochem Geophys Geosyst 2012;13(12).
[31] Bonté D, Van Wees J, Verweij JM. Subsurface temperature of the onshore Netherlands: New temperature dataset and modelling. Geol En Mijnbouw/Netherlands J Geosci 2012;91(4):491–515.
[32] Beechie T, Imaki H. Predicting natural channel patterns based on landscape and geomorphic controls in the Columbia river basin, USA. Water Resour Res 2014;50(1):39–57.
[33] Ambrose K, Hough E, Smith NJP, Warrington G. Lithostratigraphy of the sherwood sandstone group of England, Wales and south-west Scotland. 2014, Num Pages: 50 Place: Nottingham, UK Publisher: British Geological Survey.
[34] Newell AJ, Shariatipour SM. Linking outcrop analogue with flow simulation to reduce uncertainty in sub-surface carbon capture and storage: An example from the Sherwood sandstone group of the Wessex basin, UK. Geol Soc Lond Special Publ 2016;436(1):231–46.
[35] Olivarius M, Weibel R, Friis H, Boldreel LO, Keulen N, Thomsen TB. Provenance of the lower triassic bunter sandstone formation: Implications for distribution and architecture of aeolian vs. fluvial reservoirs in the north German basin. Basin Res 2017;29(S1):113–30.
[36] Kortekaas M, Böker U, Kooij C, Jaarsma B. Lower Triassic reservoir development in the northern Dutch offshore. Geol Soc Lond Special Publ 2018;469:SP469.19.
[37] Tang Z, Parnell J, Longstaffe FJ. Diagenesis and reservoir potential of Permian–Triassic fluvial/lacustrine sandstones in the southern Junggar basin, northwestern China1. AAPG Bull 1997;81(11):1843–65.
[38] Cant DJ, Walker RG. Development of a braided-fluvial facies model for the devonian battery point sandstone, Québec. Can J Earth Sci 1976;13(1):102–19.
[39] Swanson DC. The importance of fluvial processes and related reservoir deposits. J Pet Technol 1993;45(04):368–77.
[40] Gershenzon NI, Ritzi RW, Dominic DF, Mehnert E, Okwen RT, Patterson C. CO2 trapping in reservoirs with fluvial architecture: Sensitivity to heterogeneity in permeability and constitutive relationship parameters for different rock types. J Pet Sci Eng 2017;155:89–99, Energy Frontier Research Centers for Investigating Carbon Sequestration.
[41] Issautier B, Viseur S, Audigane P, Chiaberge C, Le Nindre Y-M. A new approach for evaluating the impact of fluvial type heterogeneity in CO2 storage reservoir modeling. C R Geosci 2016;348(7):531–9, Modelling Approaches in Sedimentology.
[42] Soltanian MR, Hajirezaie S, Hosseini SA, Dashtian H, Amooie MA, Meyal A, et al. Multicomponent reactive transport of carbon dioxide in fluvial heterogeneous aquifers. J Nat Gas Sci Eng 2019;65:212–23.
[43] Willems C, Nick H, Goense T, Bruhn D. The impact of reduction of doublet well spacing on the net present value and the life time of fluvial hot sedimentary aquifer doublets. Geothermics 2017;68:54–66.
[44] Ershadnia R, Wallace CD, Hajirezaie S, Hosseini SA, Nguyen TN, Sturmer DM, et al. Hydro-thermo-chemo-mechanical modeling of carbon dioxide injection in fluvial heterogeneous aquifers. Chem Eng J 2022;431:133451.
[45] Garapati N, Randolph JB, Saar MO. Brine displacement by CO2, energy extraction rates, and lifespan of a CO2-limited CO2-plume geothermal (CPG) system with a horizontal production well. Geothermics 2015;55:182–94.
[46] Randolph JB, Saar MO. Combining geothermal energy capture with geologic carbon dioxide sequestration. Geophys Res Lett 2011;38(10).
[47] Elliot TR, Buscheck TA, Celia M. Active CO2 reservoir management for sustainable geothermal energy extraction and reduced leakage. Greenh Gases Sci Technol 2013;3(1):50–65.
[48] Warren EA, Smalley CP, Howarth RJ. Part 4: Compositional variations of north sea formation waters. Geol Soc Lond Memoirs 1994;15(1):119–208.
[49] Babaei M, Nick HM. Performance of low-enthalpy geothermal systems: Interplay of spatially correlated heterogeneity and well-doublet spacings. Appl Energy 2019;253:113569.
[50] Norouzi AM, Niasar V, Gluyas JG, Babaei M. Analytical solution for predicting salt precipitation during CO2 injection into Saline aquifers in presence of capillary pressure. Water Resour Res 2022;58(6). e2022WR032612.
[51] Peng D-Y, Robinson DB. A new two-constant equation of state. Ind Eng Chem Fundam 1976;15(1):59–64, Publisher: American Chemical Society.
[52] Darcy H, Bobeck P. The public fountains of the city of dijon: exposition and application of principles to follow and formulas to use in questions of water distribution : the book ends with an appendix on water supplies of several cities' water filtration and the manufacture of cast iron, lead, and sheet metal and bitumen pipes. Kendall/Hunt Publishing Company; 2004.
[53] Willems CJ, Nick HM, Donselaar ME, Weltje GJ, Bruhn DF. On the connectivity anisotropy in fluvial hot sedimentary aquifers and its influence on geothermal doublet performance. Geothermics 2017;65:222–33.
[54] Medici G, West L, Mountney N. Characterization of a fluvial aquifer at a range of depths and scales: The Triassic St Bees sandstone formation, Cumbria, UK. Hydrogeol J 2017;26.
[55] Miall A, of Petroleum Geologists AA, of Petroleum Geologists. Fall Education Conference AA. Analysis of fluvial depositional systems. AAPG continuing education course note series, American Association of Petroleum Geologists; 1981.
[56] Sutter A. Sedimentology, depositional environments and sequence stratigraphy. 2008, URL http://www.seddepseq.co.uk/index.htm.
[57] Gibling MR. Width and thickness of fluvial channel bodies and valley fills in the geological record: A literature compilation and classification. J Sediment Res 2006;76(5):731–70.
[58] Fritsch FN, Carlson RE. Monotone piecewise cubic interpolation. SIAM J Numer Anal 1980;17(2):238–46.
[59] Babaei M, Norouzi AM, Nick HM, Gluyas J. Optimisation of heat recovery from low-enthalpy aquifers with geological uncertainty using surrogate response surfaces and simple search algorithms. Sustain Energy Technol Assess 2021.
[60] Adams BM, Kuehn TH, Bielicki JM, Randolph JB, Saar MO. A comparison of electric power output of CO2 plume geothermal (CPG) and brine geothermal systems for varying reservoir conditions. Appl Energy 2015;140:365–77.
[61] Aydin H, Merey S. Design of electrical submersible pump system in geothermal wells: A case study from west Anatolia, Turkey. Energy 2021;230:120891.
[62] Schlumberger. ECLIPSE technical description 2014.1. 2014.
[63] Pham M, Sullera M, Williams MJ, Henneberger R. ECLIPSE geothermal-a next-generation geothermal reservoir simulator. In: European geothermal congress. European Geothermal Conference; 2019.
[64] Bell IH, Wronski J, Quoilin S, Lemort V. Pure and pseudo-pure fluid thermophysical property evaluation and the open-source thermophysical property library CoolProp. Ind Eng Chem Res 2014;53(6):2498–508, Publisher: American Chemical Society.
[65] Energy UK. Energy UK. 2022, URL https://www.energy-uk.org.uk/energy-industry/watt-powers.html.
[66] Chadwick R. Offshore CO2 storage: Sleipner natural gas field beneath the north sea. In: Geological storage of carbon dioxide. Elsevier; 2013, p. 227–53e.

[67] Soltanian MR, Amooie MA, Cole DR, Graham DE, Hosseini SA, Hovorka S, et al. Simulating the cranfield geological carbon sequestration project with high-resolution static models and an accurate equation of state. Int J Greenh Gas Control 2016;54:282–96.

[68] Hovorka SD, Meckel TA, Trevino RH, Lu J, Nicot J-P, Choi J-W, et al. Monitoring a large volume CO2 injection: Year two results from SECARB project at Denbury's Cranfield, Mississippi, USA. Energy Procedia 2011;4:3478–85, 10th International Conference on Greenhouse Gas Control Technologies.

[69] Mathias SA, Gluyas JG, Mackay EJ, Goldthorpe WH. A statistical analysis of well production rates from UK oil and gas fields–implications for carbon capture and storage. Int J Greenh Gas Control 2013;19:510–8.

[70] Arnaudo M, Topel M, Puerto P, Widl E, Laumert B. Heat demand peak shaving in urban integrated energy systems by demand side management - a techno-economic and environmental approach. Energy 2019;186:115887.

[71] Xin Z, Yuxiao SUN, Di Z, Gaoxin Z, Jing LI, Xuwei W, et al. Benefit study of peak shaving energy systems using geothermal energy with storage in office buildings. Energy Storage Sci Technol 2020;9(3):720.

[72] Climate Change Committee. Reducing UK emissions, 2018 progress report to parliament. Technical report, Committee on Climate Change; 2018.

[73] Nghiem L, Sammon P, Grabenstetter J, Ohkuma H. Modeling CO2 storage in aquifers with a fully-coupled geochemical EOS compositional simulator. In: SPE/DOE symposium on improved oil recovery. Society of Petroleum Engineers; 2004.